Journal of Nano- and Electronic Physics
Vol. **14** No 3, 03001(5pp) (2022)

Журнал нано- та електронної фізики
Том **14** № 3, 03001(5cc) (2022)

Performance Study of Lead-Free Mixed Halide $Cs_2TiI_{6-x}Br_x$ (where x = 1 to 5) Based Perovskite Solar Cell

Kunal Chakraborty[1], S.V. Kumari[2], Sri Harsha Arigela[3], Mahua Gupta Choudhury[1], Sudipta Das[4], Samrat Paul[1,*]

[1] *Department of Energy Engineering, North-Eastern Hill University, Shillong, Meghalaya, India*
[2] *Department of ECE, NRI Institute of Technology, Agiripalli, Krishna Dist, AP, India*
[3] *Department of Mechanical Engineering, Koneru Lakshmaiah Education Foundation, Guntur, AP, India*
[4] *Department of ECE, IMPS College of Engineering and Technology, Nityanandapur, Malda, W.B, India*

(Received 24 May 2022; revised manuscript received 24 June 2022; published online 30 June 2022)

The present research work represents the study of device modelling and simulation of lead-free cesium titanium (IV) mixed halide ($Cs_2TiI_{6-x}Br_x$, where x = 1 to 5) based perovskite active layer. The active layer thickness, operating temperature and defect density are optimized for photovoltaic performance using SCAPS-1D (Solar Cell Capacitance Simulator – 1 Dimension) device simulator. The validity of the selection of appropriate physical and basic parameters for the proposed solar cell with cell architecture FTO/TiO_2/$Cs_2TiI_{6-x}Br_x$/CuSCN/Ag was used for the study. The optimum cell performance of the proposed device was studied for different thicknesses of the active layer, device temperature and defect density of active materials. The numerical study using SCAPS-1D revealed optimum device performance for the thickness of perovskite materials $Cs_2TiI_1Br_5$, $Cs_2TiI_2Br_4$, $Cs_2TiI_3Br_3$, $Cs_2TiI_4Br_2$, $Cs_2TiI_5Br_1$ at 1.0, 1.0, 0.4, 0.4, and 0.4 μm, respectively. The optimum device performance at temperatures of 10, 10, 20, 20, and 20 °C was numerically simulated for $Cs_2TiI_1Br_5$, $Cs_2TiI_2Br_4$, $Cs_2TiI_3Br_3$, $Cs_2TiI_4Br_2$, and $Cs_2TiI_5Br_1$ perovskite materials, respectively. The optimized defect density for all seven perovskite materials was found to be at 10^{10} cm^{-3}. The device has time of response of 1.27 μs for $Cs_2TiI_2Br_4$, $Cs_2TiI_3Br_3$, $Cs_2TiI_4Br_2$, and $Cs_2TiI_5Br_1$ absorbing layers and 1.18 μs for the $Cs_2TiI_1Br_5$ absorbing layer-based device.

Keywords: Mixed halide, Perovskite, EQE, ISA, SCAPS-1D, Photovoltaic.

DOI: 10.21272/jnep.14(3).03001 PACS numbers: 73.50.Pz, 88.40.jm

1. INTRODUCTION

The solar energy is the most effective renewable energy resource in a tropical country like India. Photovoltaic has witnessed tremendous development recently due to the discovery of new materials. Perovskite have created a huge interest among the researchers due to their unique photovoltaic properties, viz. its highly suitable optoelectronic, physical, mechanical and electrical properties like direct band gap, large charge carrier mobility, higher optical absorption coefficient and higher diffusion length makes it an ideal material for photovoltaic application [1-3]. But, due to its low shelf life and use of lead (Pb) have brought up new challenges [4-6]. The development of inorganic lead-free perovskite has created a new hope in the researchers as these materials overcome the past challenges of organic-inorganic lead-based perovskite materials [7-9]. Titanium (Ti) is an earth abundant less toxic element, and it could be a contender of replacing Pb in the perovskite structure. Ju et al. (2018) first observed, 1.0-1.8 eV tunable band gap in the cesium titanium (IV) halide perovskite materials [6]. Later, Chen et al. (2018) achieved 3.28 % power conversion efficiency (PCE) with Cs_2TiBr_6 absorbing material in the FTO/TiO_2/Cs_2TiBr_6/P3HT/Au structure [7]. Chakraborty et al. (2019) in their earlier study showed the performance of Cs_2TiBr_6, Cs_2TiI_6, Cs_2TiCl_6, Cs_2TiF_6 materials in a CdS/Cs_2TiX_6/CuSCN/Si based device structure through SCAPS-1D simulation technique [9]. The cesium titanium (IV) mixed halide perovskites are one of the best contenders for future perovskite photovoltaic device material. Thus, a detailed study of these class of materials having mixed halide perovskite ($Cs_2TiI_{6-x}Br_x$, where x = 1 to 5) is need of the hour. The present manuscript reports the numerical study for the best photovoltaic performance for optimum conditions of active layer thickness, device temperature and defect density of $Cs_2TiI_{6-x}Br_x$ perovskite material. Further, we have also studied the physical properties of the perovskite materials by the small signal impedance analysis. Impedance Spectroscopy Analysis (ISA) was than implemented using this 1D simulator to study the various physical properties like impedance (Z), capacitance (C) and conductivity (G) of the active materials were also studied. Optical properties of the materials were further investigated to discuss its absorption efficiency, direct and indirect band gap through the Tauc plot.

2. DEVICE STRUCTURE AND SIMULATION

A schematic representation of the proposed photovoltaic device FTO/TiO_2/$Cs_2TiI_{6-x}Br_x$/CuSCN/Ag is shown in Fig. 1. SCAPS-1D (Solar Cell Capacitance Simulator – 1 Dimension) software version 3.3.03 was used for the simulation. Physical parameters can be optimized through this software having a maximum of seven-layer device architecture. The effect of physical parameters viz. active layer thickness, device tempera-

* paulsamrat17@gmail.com
The results were presented at the 2nd International Conference on Innovative Research in Renewable Energy Technologies (IRRET-2022)

ture and defect density of perovskite on the performance of the proposed photovoltaic device was studied. The details of physical parameters viz. thickness, band gap (E_g), electron affinity (E_a), relative permittivity (ε_r), donor density (N_D), acceptor density (N_A), electron mobility (μ_n) and hole mobility (μ_p) for the base materials, FTO glass, ETL and HTL are shown in Table 1 [9-13]. The physical properties considered for simulation and optimization of the active layer are shown in Table 2 [12-14].

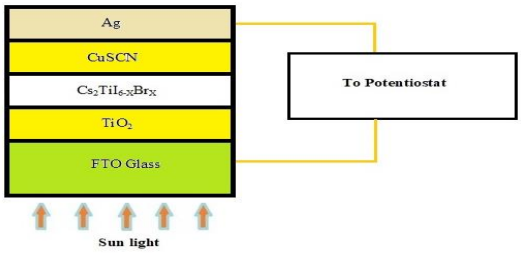

Fig. 1 – Schematic view of proposed solar cell device

Table 1 – Base material properties

Properties	CuSCN	TiO_2	FTO
Thickness (μm)	0.35	0.14	0.1
E_g (eV)	3.40	3.26	3.60
E_a (eV)	1.90	3.70	4.0
ε_r	9.0	55.0	9.0
N_D (1/cm^3)	0	4×10^{14}	2.4×10^{18}
N_A (1/cm^3)	1×10^{18}	0	1×10^{5}
μ_n (cm^2/Vs)	2×10^{-4}	100	100
μ_p (cm^2/Vs)	1×10^{-2}	25	25

Table 2 – Active material properties

Properties	I_1Br_5	I_2Br_4	I_3Br_3	I_4Br_2	I_5Br_1
Thick (μm)	0.3-3	0.3-3	0.3-3	0.3-3	0.3-3
E_g (eV)	1.58	1.38	1.26	1.15	1.07
E_a (eV)	3.42	3.62	3.74	3.85	3.93
ε_r	10	10	10	10	10
N_D (1/cm^3)	1×10^{19}	1×10^{19}	1×10^{19}	1×10^{19}	1×10^{19}
N_A (1/cm^3)	1×10^{19}	1×10^{19}	1×10^{19}	1×10^{19}	1×10^{19}
μ_n (cm^2/Vs)	4.4	4.4	4.4	4.4	4.4
μ_p (cm^2/Vs)	2.5	2.5	2.5	2.5	2.5

The active layer thickness of the perovskite is the first parameter to be optimized. The thickness of the base materials was kept fixed. The active layer ($Cs_2TiI_{6-x}Br_x$) thickness varied from 300 to 3000 nm with the device temperature to be 27 °C. The corresponding voltage-current density curves are obtained from where the other device parameters like open circuit voltage (V_{OC}), short circuit current density (J_{sc}), power conversion efficiency (PCE), fill factor (FF), and external quantum efficiency (EQE) were calculated followed by studying the optimum value of active layer thickness. The device temperature was optimized next. The optimized thickness of each active layer was taken for optimizing the temperature. The device temperature was varied from 0 to 100 °C. The optimum values of temperature and thickness obtained was used to get the optimum values of defect density. Here, the defect density is varied from 10^{10} to 10^{20} for all the seven absorbing materials and the PCE parameters were recorded to find the optimal defect density for the materials.

3. RESULTS AND DISCUSSION

3.1 Optimization of Absorbing Layer Thickness, Defect Density and Device Operating Temperature

For this study, the thickness of each perovskite active layer was varied from 300 to 3000 nm and the performance in terms of voltage and current density was recorded. The simulation results thus obtained have been used to plot V_{OC} – thickness, J_{SC} – thickness, PCE – thickness graph as shown in Fig. 2. The change in the device V_{OC}, J_{SC}, PCE can be observed for the change in the active layer thickness for all five perovskite materials viz. $Cs_2TiI_1Br_5$, $Cs_2TiI_2Br_4$, $Cs_2TiI_3Br_3$, $Cs_2TiI_4Br_2$, and $Cs_2TiI_5Br_1$. From this figure, it is clearly observed that initially with the increasing active layer thickness, the PCE values increases, and the V_{OC} falls constantly for $Cs_2TiI_1Br_5$, $Cs_2TiI_2Br_4$ absorbing layers, whereas the J_{SC} increases simultaneously after 500 nm thickness. On the other side, the V_{OC} remains constant, but J_{SC} increases with thickness variation for $Cs_2TiI_3Br_3$, $Cs_2TiI_4Br_2$, and $Cs_2TiI_5Br_1$ absorbing layers. The PCE for each perovskite material reaches maximum at a certain active layer thickness. Further, increase in the active layer thickness results in decreasing the PCE values. From Fig. 2, it is observed that for the perovskite materials $Cs_2TiI_1Br_5$ and $Cs_2TiI_2Br_4$, the PCE increases up to 1000 nm active layer thickness. Further increase in the active layer thickness results in the decrease in PCE. Similar observations are made for $Cs_2TiI_3Br_3$, $Cs_2TiI_4Br_2$ and $Cs_2TiI_5Br_1$ perovskite material where PCE increases up to a thickness of 400 nm, any increase in thickness beyond that results in decrement in the PCE value.

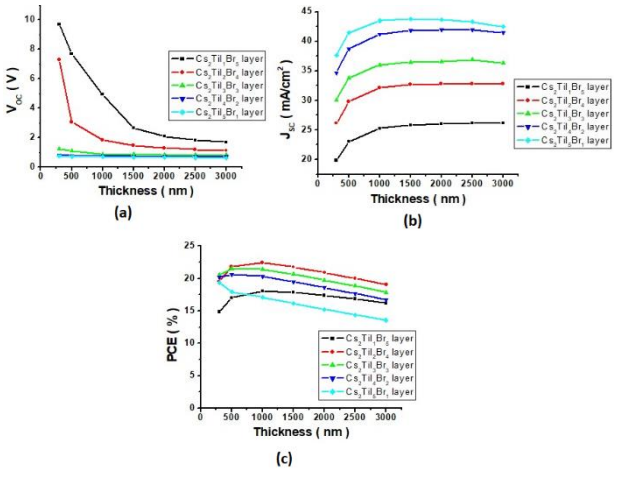

Fig. 2 – Variation of a) V_{OC}, b) J_{SC}, c) PCE with thickness for the FTO/TiO_2/$Cs_2TiI_{6-x}Br_x$/CuSCN/Ag based device structure

The probable reason for the increase in PCE with increasing the absorbing layer thickness may be due to the higher photon absorption by thicker layers [15]. At the maximum power point (MPP), the maximum power point voltage (V_{MPP}) does not change significantly with varying the thickness from 300 to 3000 nm. Whereas

the maximum power point current (I_{MPP}) has undergone a huge increment of up to 1000 nm thickness for $Cs_2TiI_1Br_5$ and $Cs_2TiI_2Br_4$ perovskite absorbing layers. Similarly, the I_{MPP} increases for $Cs_2TiI_3Br_3$, $Cs_2TiI_4Br_2$, $Cs_2TiI_5Br_1$ absorbing materials for a thickness of up to 400 nm. Such increased I_{MPP} indicates higher recombination of carriers. As a result, P_{MAX} starts to increase due to higher I_{MPP} and constant V_{MPP}. So, by analyzing all parameters, the optimized thickness for $Cs_2TiI_1Br_5$ and $Cs_2TiI_2Br_4$ materials was found to be 1000 nm. For $Cs_2TiI_3Br_3$, $Cs_2TiI_4Br_2$ and $Cs_2TiI_5Br_1$ perovskite materials, the optimum thickness was found to be 400 nm as seen from the graph. The operating temperature of the device from 0 (273) to 100 °C (373 K) was taken to optimize the device temperature. In this case, the thickness of the active layer was taken to be the optimized thickness obtained for each perovskite ($Cs_2TiI_1Br_5$ = 1.0 μm, $Cs_2TiI_2Br_4$ = 1.0 μm, $Cs_2TiI_3Br_3$ = 0.4 μm, $Cs_2TiI_4Br_2$ = 0.4 μm, $Cs_2TiI_5Br_1$ = 0.4 μm) as studied above. The decrease in V_{OC} is attributed to exponential increment in r_0^{if} in Eq. (2), which leads to similar exponential inverse increment in I_0 due to the temperature rise [16, 17]. On the other side, temperature increment may cause the increment in the recombination process which will lead to the increment in J_{SC}. It is observed that, with increase in device temperature, there is a consistent drop in V_{OC} for all the perovskite material. For $Cs_2TiI_1Br_5$ and $Cs_2TiI_2Br_4$ perovskites, there is a substantial change after 10 °C. The reason behind such peculiarities may be due to higher band gap of $Cs_2TiI_1Br_5$ (1.58 eV), and $Cs_2TiI_2Br_4$ (1.38 eV) perovskite layers. Thus, as the temperature starts to increase initially, the band gap of the materials slightly reduces leading to a drop in V_{OC} for the perovskite material. Similar observations were also observed and reported by various researchers [18, 19]. Such drop in V_{OC} results in the reduction of PCE. The variation of PCE with temperature for $Cs_2TiI_{6-x}Br_x$ absorbing perovskite layer is shown in Fig. 3. Thus, as seen from the above numerical study, the optimal temperature for $Cs_2TiI_1Br_5$ and $Cs_2TiI_2Br_4$ materials is 10 °C, whereas for $Cs_2TiI_3Br_3$, $Cs_2TiI_4Br_2$ and $Cs_2TiI_5Br_1$ materials it is 20 °C.

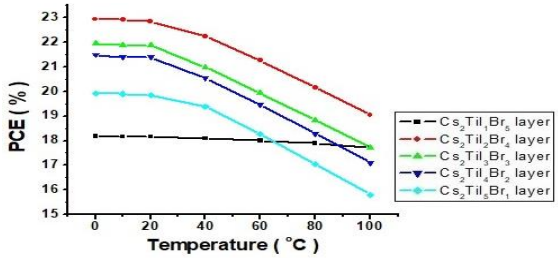

Fig. 3 – Variation of PCE with the device temperature at optimized thickness for the FTO/TiO_2/$Cs_2TiI_{6-x}Br_x$/CuSCN/Ag based device structure

Defects plays a key role in determining the performance of the photovoltaic device, as it can affect the performance of the photovoltaic device. It may cause heavy charge recombination between the interfaces [20]. The defect density (N_t, cm^{-3}) was varied from 10^{10} to 10^{20} in the Perovskite absorbing layer. For this study, the optimized values of active layer thickness and device temperatures obtained above were taken into consideration. Fig. 4 shows the variation of PCE with the change in defect density for $Cs_2TiI_{6-x}Br_x$ absorbing layer. It can be observed that the increment in defect density above 10^{10} cm^{-3} to 10^{14} cm^{-3} reduces both the PCE and P_{MAX}. The reason behind such fall in PCE and P_{MAX} may be due to the reduction in V_{OC} significantly with nominal drop of J_{SC}. A further increase in the defect density beyond 10^{14} cm^{-3}, both the V_{OC} and J_{SC} falls abruptly, thus leading to a huge reduction in the PCE and P_{MAX}. This may be due to an enormous increase in back recombination process [12, 20]. Such losses in the parameters leads to a decrease in P_{MAX}. So, it can be observed that the optimal defect density for $Cs_2TiI_{6-x}Br_x$ absorbing layer is 10^{10} cm^{-3}.

3.2 Study of External Quantum Efficiency and Optical Property

EQE is the ratio of generation of charge with respect to the illuminated photons [13]. Fig. 5 shows the effect of illumination from 100 to 1000 nm was studied for different perovskite absorbing layers.

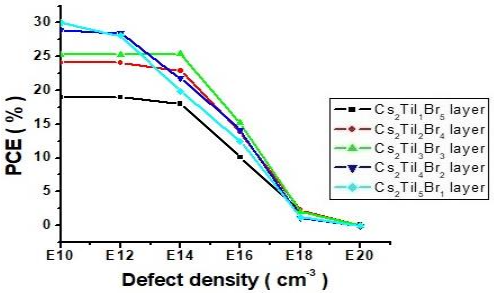

Fig. 4 – Variation of PCE with the material defect density at optimized thickness and temperature for the FTO/TiO_2/$Cs_2TiI_{6-x}Br_x$/CuSCN/Ag based device structure

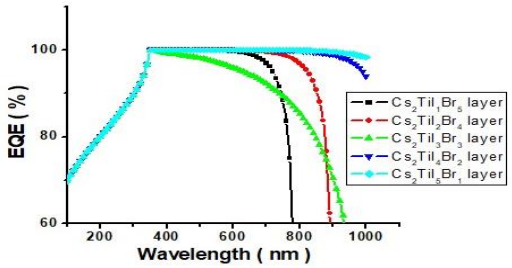

Fig. 5 – Quantum efficiency spectrum for the FTO/TiO_2/$Cs_2TiI_{6-x}Br_x$/CuSCN/Ag based device

The active materials $Cs_2TiI_1Br_5$, $Cs_2TiI_2Br_4$ and $Cs_2TiI_3Br_3$ are active up to 780 nm, 890 nm and 950 nm wavelength, whereas, other two materials $Cs_2TiI_4Br_2$, and $Cs_2TiI_5Br_1$ is seen to be active till 1000 nm wavelength. All perovskite active materials show maximum EQE at the 350 nm wavelength. The EQE starts to fall gradually from 700, 780, 450, 900, 950 nm wavelength for $Cs_2TiI_1Br_5$, $Cs_2TiI_2Br_4$, $Cs_2TiI_3Br_3$, $Cs_2TiI_4Br_2$, and $Cs_2TiI_5Br_1$ materials, respectively. This may indicate reduction in light absorbance, enhancement of reflection and low diffusion length. In the SCAPS-1D simulator, the optical absorption coefficient (α^o) can be calculated from the following model [19]. Fig. 6a shows optical absorption coefficient (α^o) spectra of different ab-

sorbing layers at the 100-800 nm wavelength. From figure it is clearly observed that at 100 nm wavelength, the value of optical absorption coefficient is almost 3.4×10^5 cm^{-1} for all the absorbing layer and after that it is fall drastically. This absorption coefficient is very important to present the Tauc plots of $\sqrt{ahv}$ and $(ahv)^2$ vs photon energy (hv) in Fig. 6b and Fig. 6c. From this figure band gaps for the indirect and direct optical transition can be easily estimated by drawing linear line in the Tauc plots. From Fig. 6b, the indirect band gap of the absorbing materials can be deduced as 1.8 eV for $Cs_2TiI_1Br_5$, 1.6 eV for $Cs_2TiI_2Br_4$, 1.55 eV for $Cs_2TiI_3Br_3$, 1.52 eV for $Cs_2TiI_4Br_2$, 1.48 eV for $Cs_2TiI_5Br_1$ approximately Whereas the direct band gap of $Cs_2TiI_1Br_5$, $Cs_2TiI_2Br_4$, $Cs_2TiI_3Br_3$, $Cs_2TiI_4Br_2$, $Cs_2TiI_5Br_1$ materials is estimated to be 1.65, 1.58, 1.44, 1.33, 1.26 eV approximately from Fig. 6c. This higher indirect band gap nature of the materials indicates that optimal photon emission efficiencies of the materials is not higher.

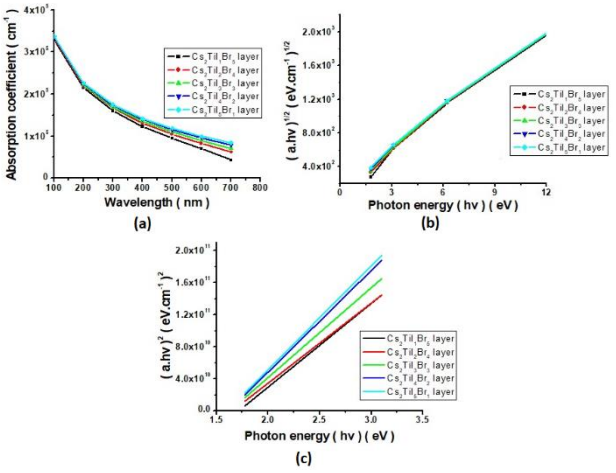

Fig. 6 – a) Absorption coefficient spectra, b) indirect optical transition, c) direct optical transition Tauc plot for the FTO/TiO_2/$Cs_2TiI_{6-x}Br_x$/CuSCN/Ag based device

3.3 Study of Impedance Spectroscopy Analysis for Perovskite Active Layers

Impedance spectroscopy analysis (ISA) is an advanced technique to study the active material properties which allows the characterization of materials in a large range scale of higher and lower frequencies [20]. In this technique, an AC signal (small frequency modulated frame) is applied to a DC signal. ISA helps to characterize kinetic processes of active materials with respect to different time scale. Nyquist plot and Bode plot are two tools which is very useful to analyze the complex frequency dependent impedance characteristics [18]. Here, the real and imaginary parts of the impedance (Z, Ohm) are described in the x-axis and y-axis, respectively. In Fig. 7a and Fig. 7b, the Nyquist plot and Bode plot of the perovskite solar cell device at the optimized conditions is depicted in the frequency frame. By looking in Fig. 7a, it can be seen that the Nyquist plot arc for the $Cs_2TiI_2Br_4$, $Cs_2TiI_3Br_3$, $Cs_2TiI_4Br_2$, and $Cs_2TiI_5Br_1$ perovskite materials are almost similar, and the device has a deteriorated semi-circular shape. On the other side, $Cs_2TiI_1Br_5$ absorbing layer has near perfect semi-circular shape. The semi-circular shape obtained due to the parallel formation of RC pair (where R is shunt resistance and C is the junction capacitance of the device). The perovskite solar cells produce an arc, which are slightly different from the semi-circular shape, this may be due to the AC in the device [20]. The reason behind the slight deviation from semi-circular shape of the arc may also be attributed to the existence of multiple reactive behavior in the different interfaces of the device. On the other side, the Bode plot shows a peak at 0.125 MHz frequency for all the materials except the $Cs_2TiI_1Br_5$, where peak is observed at 0.135 MHz. By reversing the peak frequency, the characteristic time (resonance time) of the device can be easily found. So, the corresponding resonance time period for $Cs_2TiI_2Br_4$, $Cs_2TiI_3Br_3$, $Cs_2TiI_4Br_2$, and $Cs_2TiI_5Br_1$ absorbing layer based devices is approximately 1.27 µs, and for the $Cs_2TiI_1Br_5$ material based device is 1.18 µs. This faster response of the device indicates pure electronic changes has occurred in the device. The capacitance (C) – voltage (V) and conductance (G) – voltage (V) graphs are very useful for the estimation of total radiation induced in the solar cell. Fig. 7c and Fig. 7d show the C-V and G-V plots for different perovskite materials. From this graph, it is clearly visible that both C and G are varying with the applied voltage, and it is also observed that highest peak in the C-G plot is same for the $Cs_2TiI_1Br_5$, $Cs_2TiI_2Br_4$, $Cs_2TiI_3Br_3$ perovskite layers at 0.78, 0.72 and 0.7 V, respectively, whereas for the other perovskite materials there is a significant difference in the C-G plot with V. The reason behind this variation may be due to the existence of impurity with the lower frequency level of the impedance.

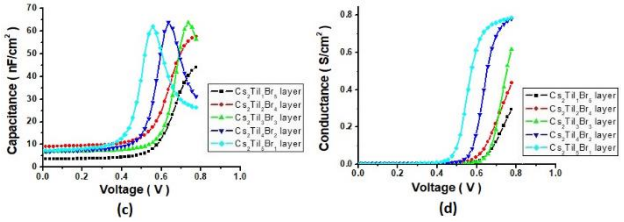

Fig. 7 – Impedance analysis: a) Nyquist plot, b) Bode plot, c) C-V plot, d) G-V plot for the FTO/TiO_2/$Cs_2TiI_{6-x}Br_x$/CuSCN/Ag based device

4. CONCLUSIONS

This research article presents the optimization of thickness of absorbing layer, device temperature and material defect density for $Cs_2TiI_{6-x}Br_x$ perovskite material. The performance of the device in terms of PCE, J-V, P_{MAX}, FF, and EQE obtained using the simulation was used to study the optimized condition for the parameters. The optimum device performance is observed at 1.0, 1.0, 0.4, 0.4, and 0.4 µm for $Cs_2TiI_1Br_5$, $Cs_2TiI_2Br_4$, $Cs_2TiI_3Br_3$, $Cs_2TiI_4Br_2$, and $Cs_2TiI_5Br_1$ perovskite materials, respectively. Whereas the optimum device temperatures are found to be at 10, 10, 20, 20, 20 °C for $Cs_2TiI_1Br_5$, $Cs_2TiI_2Br_4$, $Cs_2TiI_3Br_3$, $Cs_2TiI_4Br_2$, and $Cs_2TiI_5Br_1$ perovskite materials, respectively. During the simulation process, it was observed that defect density had a great impact on the charge recombination

rate. The optimized defect density of 10^{10} cm^{-3} is observed to be optimal for all five absorbing materials. The $Cs_2TiI_1Br_5$ absorbing material-based device has better Nyquist shape and faster time of response with resonance time period of 1.18 μs. This indicates, $Cs_2TiI_1Br_5$ absorbing material based device has better opto-electrical property compared to other four material.

ACKNOWLEDGEMENTS

The authors are grateful to the Department of Electronics and Information Systems, University of Gent, Belgium and Prof. Burgelman for providing the SCAPS software to carry out this research work. The authors are also thankful to the Science and Engineering Research Board (SERB), Department of Science and Technology (DST) India for their financial support (EMR/2016/002430) to carry out this research work.

REFERENCES

1. A. Kojima, K. Teshima, Y. Shirai, T. Miyasaka, *J. Am. Chem. Soc.* **131** No 17, 6050 (2009).
2. F. Giustino, H.J. Snaith, *ACS Energy Lett.* **1** No 6, 1233 (2016).
3. S.D. Stranks, G.E. Eperon, G. Grancini, C. Menelaou, M.J. Alcocer, T. Leijtens, L.M. Herz, A. Petrozza, H.J. Snaith, *Science* **342** No 6156, 341 (2013).
4. W.S. Yang, J.H. Noh, N.J. Jeon, Y.C. Kim, S. Ryu, J. Seo, *Science* **348** No 6240, 1234 (2015).
5. W.J. Yin, J.H. Yang, J. Kang, Y. Yan, S.H. Wei, *J. Mat. Chem. A* **3** No 17, 8926 (2015).
6. M.G. Ju, M. Chen, Y. Zhou, H.F. Garces, J. Dai, L. Ma, N.P. Padture, X.C. Zeng, *ACS Energy Lett.* **3** No 2, 297 (2018).
7. M. Chen, M.G. Ju, A.D. Carl, Y. Zong, R.L. Grimm, J. Gu, X.C. Zeng, Y. Zhou, N.P. Padture, *Joule* **2** No 3, 558 (2018).
8. S. Paul, S. Grover, I.L. Repins, B.M. Keyes, M.A. Contreras, K. Ramanathan, R. Noufi, Z. Zhao, F. Liao, J.V. Li, *IEEE J. of Photovolt.* **8** No 3, 871 (2018).
9. K. Chakraborty, M.G. Choudhury, S. Paul, *Sol. Energy* **194** No 12, 886 (2019).
10. S.K. Pandey, S. Somay, *IEEE Trans. Electron Dev.* **67** No 10, 4321 (2020).
11. N. Rai, S. Rai, P.K. Singh, P. Lohia, D.K. Dwivedi, *J. Mat. Sci: Mat. Elec.* **31** No 19, 16269 (2020).
12. K. Chakraborty, S. Paul, U. Mukherjee, S. Das, *J. Nano-Electron. Phys.* **13** No 3, 03009 (2021).
13. K. Chakraborty, M.G. Choudhury, S. Paul, *IEEE Trans. Dev. Mat. Reliab.* **21** No 4, 465 (2021).
14. K. Tan, P. Lin, G. Wang, Y. Liu, Z. Xu, Y. Lin, *Solid-State Electron.* **126** No 12, 75 (2016).
15. K. Chakraborty, M.G. Choudhury, S. Paul, *IEEE J. Photovolt.* **11** No 2, 386 (2021).
16. N. Chaudhary, R. Chaudhary, *J. Mat. Chem. C* **3** No 45, 11886 (2015).
17. Y. Yang, J. You, *Nature* **544** No 4, 155 (2017).
18. A. Zhang, Y. Chen, J. Yan, *IEEE J. Quan. Electron.* **52** No 6 (2016).
19. Shubham, Raghvendra, C. Pathak, S.K. Pandey, *IEEE Trans. Electron. Dev.* **67** No 7, 2837 (2020).
20. I. Matacena, L. Lancellotti, N. Lisi, P.D. Veneri, P. Guerriero, S. Daliento, *Energies* **13** No 8, 1908 (2020).

Дослідження ефективності перовскітного сонячного елементу на основі безсвинцевого змішаного галогеніду $Cs_2TiI_{6-x}Br_x$ (x = 1 до 5)

Kunal Chakraborty[1], S.V. Kumari[2], Sri Harsha Arigela[3], Mahua Gupta Choudhury[1], Sudipta Das[4], Samrat Paul[1]

[1] *Department of Energy Engineering, North-Eastern Hill University, Shillong, Meghalaya, India*
[2] *Department of ECE, NRI Institute of Technology, Agiripalli, Krishna Dist, AP, India*
[3] *Department of Mechanical Engineering, Koneru Lakshmaiah Education Foundation, Guntur, AP, India*
[4] *Department of ECE, IMPS College of Engineering and Technology, Nityanandapur, Malda, W.B, India*

Дана науково-дослідна робота являє собою дослідження моделювання пристрою та імітації перовскітного активного шару на основі безсвинцевого змішаного галогеніду цезію-титану (IV) ($Cs_2TiI_{6-x}Br_x$, де x = 1 до 5). Товщина активного шару, робоча температура та густина дефектів оптимізовані для фотоелектричних характеристик за допомогою симулятора пристрою SCAPS-1D (Solar Cell Capacitance Simulator – 1 Dimension). Для дослідження використано обґрунтованість вибору відповідних фізичних та базових параметрів запропонованого сонячного елемента з архітектурою FTO/TiO_2/$Cs_2TiI_{6-x}Br_x$/CuSCN/Ag. Досліджено оптимальні характеристики елементів пропонованого пристрою для різних товщин активного шару, температури пристрою та густини дефектів активних матеріалів. Чисельне дослідження з використанням SCAPS-1D показало оптимальну продуктивність приладу для товщин перовскітних матеріалів $Cs_2TiI_1Br_5$, $Cs_2TiI_2Br_4$, $Cs_2TiI_3Br_3$, $Cs_2TiI_4Br_2$ та $Cs_2TiI_5Br_1$, відповідно рівних 1,0; 1,0; 0,4; 0,4 та 0,4 мкм. Оптимальну продуктивність приладу при температурах 10, 10, 20, 20 та 20 °C чисельно моделювали для перовскітних матеріалів $Cs_2TiI_1Br_5$, $Cs_2TiI_2Br_4$, $Cs_2TiI_3Br_3$, $Cs_2TiI_4Br_2$ та $Cs_2TiI_5Br_1$ відповідно. Встановлено, що оптимізована густина дефектів для всіх семи перовскітних матеріалів становить 10^{10} см$^{-3}$. Пристрій має час відгуку 1,27 мкс для поглинаючих шарів $Cs_2TiI_2Br_4$, $Cs_2TiI_3Br_3$, $Cs_2TiI_4Br_2$ і $Cs_2TiI_5Br_1$ та 1,18 мкс для пристрою на основі поглинаючого шару $Cs_2TiI_1Br_5$.

Ключові слова: Змішаний галогенід, Перовскіт, EQE, ISA, SCAPS-1D, Фотоелектричний.